

Bayesian Geoacoustic Inversion With the Image Source Method

Laurent Guillon, Stan E. Dosso, N. Ross Chapman, *Fellow, IEEE*, and Achraf Drira

Abstract—This paper develops a Bayesian approach to the image source method (ISM) for efficient inversion of seabed reflection data to estimate geoacoustic parameters and uncertainties. Based on the representation of layered seafloor-reflected signals by image sources, ISM is a very efficient method which provides the local sound-speed profile (SSP) of the sediment structure. It is a two-step method: first, the image sources are detected and localized from the recorded signals, and second, from these locations, the thickness and sound speed of each sediment layer are estimated from the Snell–Descartes law of refraction. This work focuses on the definition and construction of the image sources with a distinction between real and virtual image sources which has consequences on the uncertainties of ISM. The localization of the image sources is performed within a Bayesian formulation based on sampling the posterior probability density to estimate the median SSP and uncertainties. The algorithm is tested first on synthetic data, with results in excellent agreement with Bayesian travel-time inversion but a much lower computational cost. Finally, the Bayesian ISM is applied to at-sea data measured in the Scattering And Reverberation from the sea Bottom (SCARAB) experiment, which took place near Elba Island off the west coast of Italy in 1998, and the resultant sediment SSP agrees well with previous results of other geoacoustic inversion methods.

Index Terms—Bayesian methods, geoacoustic inversion, image sources, Teager–Kaiser energy operator, travel-time detection.

I. INTRODUCTION

THIS paper deals with geoacoustic inversion in the mid-frequency range, around a few kilohertz. Using this frequency range provides both sufficient signal penetration and spatial resolution to infer properties of a layered sub-bottom structure on the scale of 10^{-1} to 10^1 m, which is important for many sonar applications. Seafloor characterization by acoustics can be achieved through a variety of strategies: analysis of sidescan sonar or multibeam echosounder reflectivity maps, matched-field processing, analysis of scattered or reflected signals, and passive acoustics, to list a few (see, e.g., [1] or [2] and references therein). The method presented and further developed in this paper is a recent one, based on the analysis of an acoustic signal reflected by the seafloor and is called the image

Manuscript received April 14, 2015; revised October 16, 2015; accepted January 04, 2016. Date of publication February 18, 2016; date of current version October 11, 2016. The work of L. Guillon was supported in part by the Délégation Générale de l'Armement (DGA) under Grant ERE 2013.60.0012.

Associate Editor: N. Chotiros.

L. Guillon is with the Research Institute of the French Naval Academy, 29240 Brest Cedex 9, France. He was with the School of Earth and Ocean Sciences, University of Victoria, Victoria, BC V8W 3P6 Canada (e-mail: laurent.guillon@ecole-navale.fr).

S. E. Dosso and N. R. Chapman are with the School of Earth and Ocean Sciences, University of Victoria, Victoria, BC V8W 3P6 Canada.

A. Drira is with the Research Institute of the French Naval Academy, 29240 Brest Cedex 9, France.

Digital Object Identifier 10.1109/JOE.2016.2516421

source method (ISM). It provides the local sound-speed profile (SSP) of layered seafloors with good resolution and at a low computational cost [3]–[5] allowing near-real-time analysis.

In inverse problem studies, statistical approaches have been developed for more than two decades (see, e.g., [6] and references therein). The essential idea is that the model parameters that are sought from experimental data are considered random variables and described by their posterior probability density (PPD). Instead of estimating a single optimal value for the model parameters, the PPD of the model is estimated, providing complete knowledge of the parameter statistics. These methods inherently take into account the uncertainties, not only from experimental measurements, but also due to the forward modeling. Therefore, they are powerful methods but their main drawback is that they can require large computation times. The main objective of the present work is to combine the simplicity and efficacy of the ISM with the generality of the Bayesian approach for efficient reflection travel-time inversion.

The paper is organized in four sections. First, the ISM principle is reviewed, with a focus on the forward modeling approximations. Second, image sources detection and localization are presented and the Bayesian approach is developed. Third, the inversion and ISM algorithms are presented. Fourth, the new Bayesian ISM algorithm is applied to synthetic and real data and the results are discussed.

II. PRINCIPLE OF THE IMAGE SOURCE METHOD

A. Principle

The ISM is based on analysis of the reflection of a broadband acoustic signal emitted by a point source above a layered seafloor and recorded by a hydrophone array [see Fig. 1(a)]. Three hypotheses are made:

- 1) the sediment layers are fluid and homogeneous, and the interfaces are parallel;
- 2) the incident angle on the layer interfaces is below the critical incident angle;
- 3) the multiple reflections inside the sediment stack can be neglected.

Under these hypotheses, the signal reflected by the layered seafloor can be modeled as being emitted by image sources, symmetric to the real source relative to the reflecting interfaces. Therefore, the layered seafloor can be represented by an equivalent system where the layer thicknesses are doubled and the image sources are placed on the interfaces [see Fig. 1(b)]. In this system, the amplitudes of the received signals require corrections, but in the ISM, this information is not used. The method

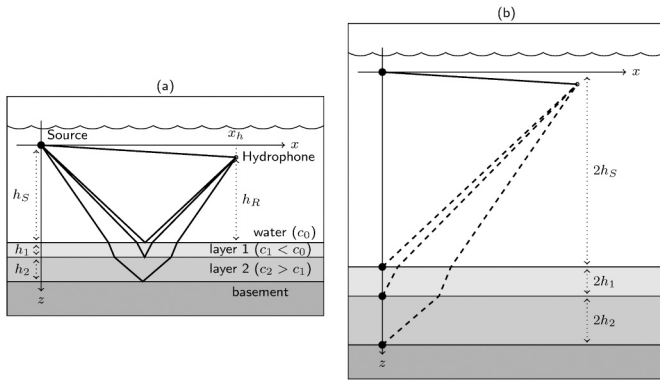


Fig. 1. (a) Reflection of a point source signal by a two-layer seafloor. (b) Modeling of this situation by image sources.

is only based on travel-time information and, in the equivalent system, the arrival angle and the travel time of the various arrivals are exactly the same as in the real configuration.

The locations of the image sources are linked directly to the SSP of the layered seafloor. Therefore, the idea of the ISM is to detect and localize the image sources in order to infer the SSP. Since we want to localize the image sources only from the recorded time signals, it is necessary to use an array of hydrophones. The array processing used here is explained in Section III, but it has some consequences that are first explained below.

A. “Real” and “Virtual” Image Sources

If the seafloor SSP is known, the refraction process can be taken into account and the image sources can be placed exactly on the interfaces and on the vertical axis below the source [black dots at the ends of dashed lines in Fig. 1(b) and of dotted lines in Fig. 2]. But, in the context of geoaoustic inversion, this profile is what we seek and is thus unknown. So, instead of dealing with the “real” image sources, the recorded signals are modeled as being emitted by “virtual” image sources representing the source positions that match the measured travel times and arrival angles at a hydrophone location if the entire medium is homogeneous water, i.e., when acoustic rays are straight lines. These virtual sources are no longer located on the image interfaces, nor on the vertical axis below the source (+ symbols in Fig. 2).

The SSP inversion algorithm of ISM is based on knowledge of the travel time t and arrival angle θ between two points (see Section IV-A and Fig. 2): a single receiver and a virtual image source corresponding to a given layer. This leads to two difficulties. The first problem is to define an equivalent receiver for the hydrophone array at a position such that all the quantities t and θ are defined. In the following, the median position of all the hydrophone positions is used for this purpose.

The second problem deals with the nonuniqueness of each individual virtual image source. Indeed, the locations of the real image sources (on the interfaces directly below the source) are independent of the hydrophone position; they only depend on the thicknesses of the seafloor layers. But this is not the

case for the virtual image sources as their locations do depend on the hydrophone position. Therefore, when the signals are recorded on an array, an image source is not seen as a single point but rather as a cloud of points with a shape and a spatial extent that depends on the shape and length of the hydrophone array (see Fig. 3). This leads to an inherent compromise of the ISM: to locate the image sources, one needs to use multiple hydrophones instead of a single receiver, but this implies that the image source is not a single point but a cloud of points. The original situation illustrated in Fig. 2 becomes, in practice, that shown in Fig. 3: for an array of N_h hydrophones, there are N_h virtual image sources instead of a single one for a given layer. The problem of defining an equivalent virtual image source from these N_h virtual image sources is addressed in Section III.

A. Forward Modeling

Assuming that an N -layer seafloor above a semi-infinite basement provides $N_S = N + 1$ image sources, the reflected signals recorded on an array composed of N_h hydrophones lead to $N_t = N_S \times N_h$ travel times from source to hydrophones. The forward modeling of ISM converts the N_t travel times into $2N_S$ data which are the pairs $t^{(i)}$ and $\theta_0^{(i)}$ for each layer. This drastic reduction in the number of data to invert explains the low computational cost of ISM.

It should be noted that in inverse problem theory, two types of uncertainties can be defined which are due to errors from data measurements and from modeling procedures. Modeling errors in ISM arise from the process of defining a single equivalent virtual image source from the cloud of all virtual image sources (see Fig. 3).

Another way of inferring the SSP from the experimental configuration depicted in Fig. 1 is to use all the N_t travel times as data for a ray-based Bayesian inversion method (see, e.g., [7]). This is described in Section V and used there as a comparison for ISM results.

III. IMAGE SOURCES DETECTION AND LOCALIZATION

An earlier algorithm used for the detection and location of image sources is based on array processing and seismic techniques [4], [8]. The idea of that algorithm is to migrate the recorded signals in water so as to focus the image sources. Since the focus is not perfect, a semblance map is also computed which ideally gives a value of unity at image-source locations and zero elsewhere. A mask is built on the semblance map where its value is above a given threshold and the maxima of the migration map are picked on this mask, giving the locations of the image sources. Finally, the travel time $t^{(i)}$ and arrival angles $\theta_0^{(i)}$ are computed from these locations and the center of the array taken to be its median position (Fig. 2).

In this paper, we use a different technique which is split in two parts: arrival-time detection with the Teager–Kaiser energy operator (TKEO), and image-source localization through a Bayesian approach. In this new approach, no array processing such as beamforming or migration is used.

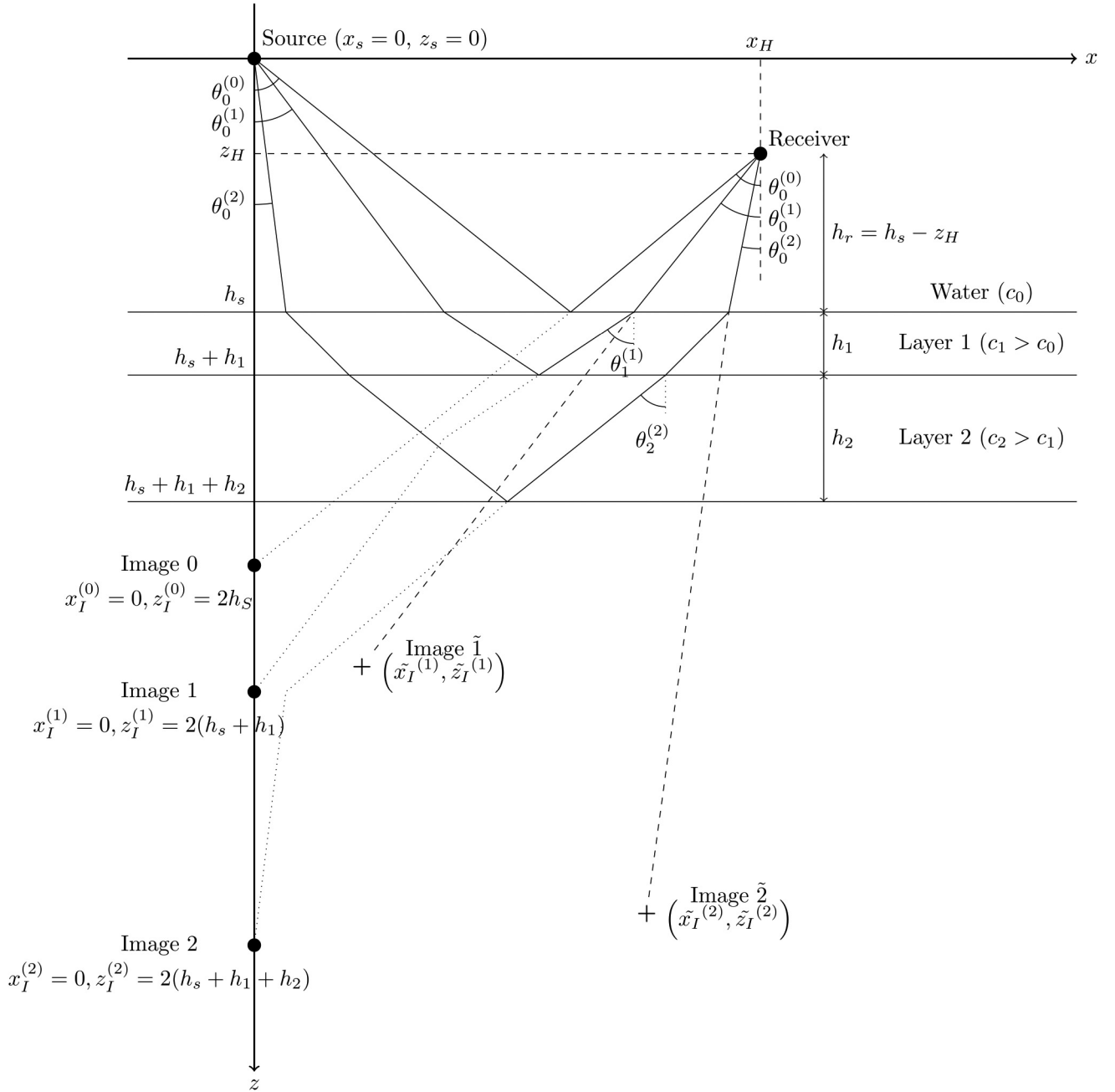


Fig. 2. Geometry for the “real” (filled circles) and “virtual” (+ symbols) image sources in the case of a SSP that increases with z . The dotted lines represent the refracted acoustic path (from the real image sources to the receiver) whereas the dashed lines do not include refraction.

B. Arrival-Time Detection With TKEO

The idea is to use the TKEO [9] to detect precisely the arrival times of reflections at each hydrophone [5], [10]. In continuous time, the TKEO is defined as

$$\Psi[x(t)] = \dot{x}(t)^2 - x(t)\ddot{x}(t) \quad (1)$$

where the dot indicates time differentiation. For a discrete time signal x_n , the TKEO can be approximated as follows [11]:

$$\Psi[x_n] = x_n^2 - x_{n+1}x_{n-1}. \quad (2)$$

Equation (2) shows that the TKEO computes a running estimate of the signal energy at each instant that takes into account

the signal strengths at the neighboring instants. An important aspect of the TKEO is that it amplifies discontinuities and sudden changes in amplitude while smooth transitions between the samples are reduced. This property is mainly attributed to the use of second-order derivative and is exploited here for the estimation of arrival times by identification of peaks in the TKEO output.

To detect peak arrivals in the recorded signals for each hydrophone, the following algorithm is used:

- 1) cross correlation of the recorded signals with the emitted signal (when available) and normalization of the results;
- 2) interpolation if the sampling frequency is too low;

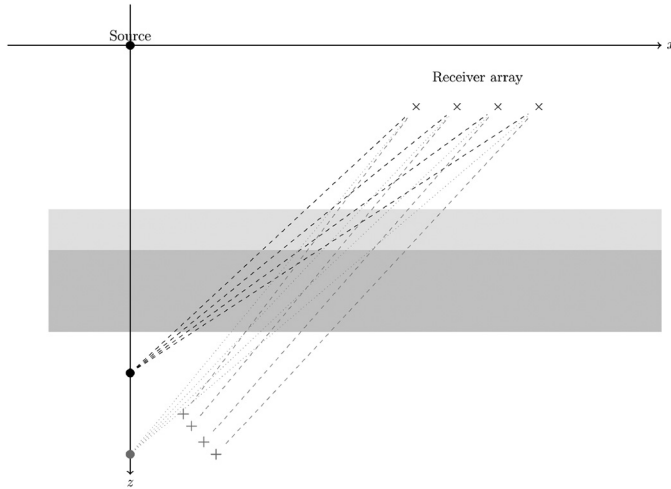


Fig. 3. Two first real and virtual image sources of Fig. 2 for a receiving array.

- 3) Savitzky–Golay (SG) filtering (local polynomial regression [12]) to smooth the signal after oversampling;
- 4) TKEO computation and SG filtering of the result;
- 5) peak detection.

Concerning the last point, the peak detection is controlled by a threshold. It has been shown [5], at least on synthetic data, that this threshold can be computed from the data instead of being set by the user.

The first step of the detection algorithm (cross correlation) depends on knowledge of the emitted signal waveform and on the synchronization of the emitted and received signals. For synthetic signals, this knowledge is obviously available, but for data acquired at sea, even if the emitted signal is known or deduced from recordings, the source and receivers are rarely synchronized, at least with sufficient accuracy. In this case, the travel-time detection is divided in two parts. First, we use the TKEO to detect the two first arrivals in the signal. In this work, we consider that the source and the array are at a depth such that the sea-surface-reflected path arrives after the direct and the seafloor-interface-reflected path and can be therefore eliminated. This rejection could also be done by considering the phase reversal of the sea-surface-reflected path. So, the two first arrivals correspond to the direct path and the seafloor-interface-reflected path. Since these two paths propagate only in water, and assuming that we know the propagation geometry (position of source and receivers) and water sound speed, their travel times can be computed theoretically. The difference between the theoretical and estimated values gives the source emission time t_0 . After that, the detection algorithm is applied to the signals where the direct path has been removed. The obtained arrival times are corrected by the emission time t_0 to finally provide the travel times $t^{(i)}$ for each detected image source.

After this step, we have $N_s \times N_h$ travel times, corresponding to the reflections at each layer interface as recorded at each hydrophone. Since these paths correspond to straight-line propagation from each virtual source to each hydrophone in homogeneous water, this corresponds directly to the situation sketched in Fig. 3.

In a recent work [5], it has been proposed to use a triangulation process to locate the image sources from all the

detected travel times. In this present paper, we propose another method, based on a Bayesian sampling approach. Once the image sources are located, the angles required by the next step of the inversion algorithm are easily computed from these locations and the median of the hydrophone locations.

B. Bayesian Localization of Image Sources

The starting point here is to consider that we are seeking the median position $(x^{(i)}, z^{(i)})$ of virtual image sources of a particular layer i and that $t_k^{(i)}$ with $k \in [1..N_h]$ are the travel times between the hydrophones and this median position. This median position defines the equivalent virtual image source which is used in the inversion algorithm (see Section IV-A). The virtual image sources are defined in a homogeneous medium with sound speed c_0 ; hence, these travel times are converted directly into distances $d_k^{(i)}$. In this section, we omit the superscripts (i) for convenience.

The model parameters to be determined at this stage are the coordinates of the equivalent virtual image source: $\mathbf{m} = (x, z)$. The data are the arrival travel times: $\mathbf{d} = \{t_k\}$ with $k \in [1..N_h]$.

The forward model $\mathbf{d} = \mathbf{g}(\mathbf{m})$ is simply solved by the following system of equations:

$$t_k = g_k(x, z) = \frac{1}{c_0} \sqrt{(x - X_k)^2 + (z - Z_k)^2} \quad (3)$$

with $k \in [1..N_h]$ and where X_k and Z_k are the coordinates of the hydrophones.

The objective is to obtain the posterior probability density (PPD) expressed in Bayes' theorem

$$P(\mathbf{m}|\mathbf{d}) = \frac{P(\mathbf{d}|\mathbf{m})P(\mathbf{m})}{P(\mathbf{d})}. \quad (4)$$

Once the experiment has been carried out and the data obtained, $P(\mathbf{d})$ is a constant factor which can be absorbed into the normalization, and the conditional probability density function (pdf) $P(\mathbf{d}|\mathbf{m})$ can be interpreted as a function of \mathbf{m} known as the likelihood function. If we assume that the errors on the data are independent and Gaussian distributed with standard deviation σ_t , this likelihood function can be written as

$$L(x, z) \propto \exp \left[-\frac{1}{2\sigma_t^2} \sum_{k=1}^{N_h} (t_k^{\text{cal}}(x, z) - t_k^{\text{obs}})^2 \right] \quad (5)$$

where the travel times t_k^{cal} are obtained by the forward model and the travel times t_k^{obs} by applying the TKEO detection algorithm to recorded acoustic time series.

By construction, the virtual image sources are located around the vertical axis below the real source. To define a relatively uninformative prior, the prior pdf $P(\mathbf{m})$ is set to a uniform probability distribution within a box surrounding this vertical axis.

The PPD $P(\mathbf{m}|\mathbf{d})$ is obtained through the Metropolis–Hastings sampling algorithm (see, e.g., [13] or [14]). This gives N_{samp} samples of the PPD consistent with (4). The equivalent virtual image source can be defined from these samples, for example, by taking their median or mean position. With this equivalent position, we can compute the input parameters needed by the inversion algorithm. Further, each sample

of virtual image source locations drawn from the PPD via the Metropolis–Hastings algorithm can be inverted to produce a sample of the SSP for the seabed sediment layers as described in Section IV-A. The resulting ensemble of these samples defines the SSP PPD and can be used to quantify the SSP uncertainty (see Section IV-B).

IV. INVERSION ALGORITHM

C. SSP Inversion

The data processing described in Section III provides:

- the number of image sources N_s ;
- the travel times $t^{(i)}$ with $i \in [0, \dots, N_s - 1]$ for each equivalent virtual image source to the equivalent receiver;
- the incident angles $\theta_0^{(i)}$ for each equivalent virtual image source at the equivalent receiver.

In the above statement, the “equivalent receiver” and the “equivalent virtual image source” are defined as in Sections II-B and III-B. Further necessary information includes:

- the position of the source, which is taken as the origin of the coordinate system;
- the position of the receiver (x_H, z_H) ;
- the height of the source above the seafloor, h_s ;
- the water sound speed c_0 .

With this information and the $2 \times N_s$ data $(t^{(i)}, \theta_0^{(i)})$, the inversion algorithm is quite straightforward and is based only on the Snell–Descartes law of reflection and refraction. It acts in a recursive way. The estimated quantities are denoted \tilde{c} , the estimated layer sound speed, and \tilde{e} , the layer thickness (cf., Fig. 1). The algorithm is initialized with $\tilde{c}_0 = c_0$ and $\tilde{e}_0 = 2h_s - z_H$.

The first image source (image 0 in Fig. 2) does not provide information about the seafloor unless the amplitude of the signals is used, which is not the case here. Nevertheless, it can be used to provide information about the geometry of the experiment, particularly for the array shape [4]. In this paper, the time of arrival of this first image source is used jointly with the time of arrival of the direct signal to infer the time of signal emission in cases where this is unknown.

Let us consider that we have already inverted for the SSP down to layer $i - 1$. From the arrival time $t^{(i)}$ and arrival angle $\theta_0^{(i)}$ of image source i , we first compute the incident angle in layer $i - 1$

$$\theta_{i-1}^{(i)} = \arcsin \left(\tilde{c}_{i-1} \sin \theta_0^{(i)} / c_0 \right). \quad (6)$$

From this, the travel time in layer i is obtained by subtracting the sum of the travel times in the above layers from the total travel time

$$t_s^{(i)} = t^{(i)} - \sum_{k=0}^{i-1} \frac{\tilde{e}_k}{\tilde{c}_k \cos \theta_k^{(i)}}. \quad (7)$$

With the help of the Snell–Descartes refraction law, the sound speed in layer i is finally estimated by

$$\tilde{c}_i = \sqrt{\frac{c_0}{t_s \sin \theta_0^{(i)}} \left[x_H - \sum_{k=0}^{i-1} \tilde{e}_k \tan \theta_k^{(i)} \right]} \quad (8)$$

and the equivalent thickness is obtained by

$$\tilde{e}_i = \tilde{c}_i t_s \cos \left[\arcsin \left(\frac{\tilde{c}_i \sin \theta_0^{(i)}}{c_0} \right) \right]. \quad (9)$$

The algorithm is repeated recursively until the last virtual image which gives the parameters of layer $N_s - 1$.

C. ISM Algorithm

The ISM can be summarized as a two-step algorithm.

- 1) From the recorded signals, the number N_s of image sources is obtained together with the travel time $t^{(i)}$ and arrival angle $\theta_0^{(i)}$ between each equivalent virtual image and the equivalent receiver. This point is described in Section III.
- 2) From these inputs and the preliminary information given in Section IV-A, the sediment SSP is obtained through (6)–(9).

When this algorithm is applied with one equivalent virtual image source for each layer, it provides one SSP estimation for the seafloor. These were the results presented in previous works [3]–[5]. But in the present work, at the end of the first step (described in Section III), we have N_{samp} samples of the (x, z) positions of all virtual image sources drawn from the PPD for image sources locations by the Metropolis–Hastings sampling algorithm. The SSP can be estimated from each sample of virtual image sources using the algorithm presented in Section IV-A, yielding a sampled PPD for the SSP. In this procedure, lower and upper bounds are set on \tilde{c} and \tilde{e} to avoid unrealistic SSP. Finally, a median SSP and SSP uncertainties can be computed from this PPD.

V. RESULTS

A. Synthetic Data

To test the proposed approach, the algorithm is first applied to synthetic data computed by the software `specfem2D`¹ which is a spectral element code developed to simulate seismic-wave propagation at the Earth scale [15]. Recently, this software has been applied to underwater acoustics problems [16] and to T-wave generation and propagation modeling [17].

The geometric configuration of the synthetic example is inspired by the Clutter09 experiment [18]: a broadband acoustic source is towed at a height of 12 m over the seafloor ahead of a towed horizontal line array (HLA) comprising 15 hydrophones regularly spaced with a separation of 1 m. The distance between the source and the first hydrophone of the HLA is 24 m. The sound speed in the water is set at 1500 m/s. The use of a towed source and HLA instead of using a moored array [3] allows the ISM to invert for range-dependent seafloors [4], although this is not done here.

Three different geoacoustic configuration are used (Table I). The first case is very simple with only two layers over a basement. In the second case, a layer with sound speed lower than

¹This software is available at: <http://geodynamics.org/cig/software/specfem2d/>

TABLE I

GEOACOUSTIC PARAMETERS FOR THE THREE CONFIGURATIONS USED FOR SYNTHETIC DATA. IN ALL CASES, BASEMENT SOUND SPEED IS 2000 m/s

Name	# layers	c_1 (m/s)	h_1 (m)	c_2 (m/s)	h_2 (m)	c_3 (m/s)	h_3 (m)	c_4 (m/s)	h_4 (m)	c_5 (m/s)	h_5 (m)
Config1	2	1650	2	1750	2	-	-	-	-	-	-
Config2	3	1480	1	1650	2	1750	2	-	-	-	-
Config3	5	1480	0.5	1527	1	1660	6	1960	1	1660	4

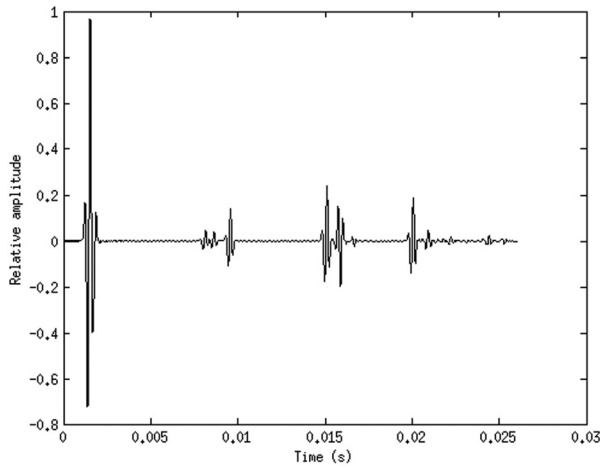


Fig. 4. Signal at the first hydrophone for Config3. The first arrival corresponds to the direct path while the latter arrivals are reflections from the seafloor interfaces.

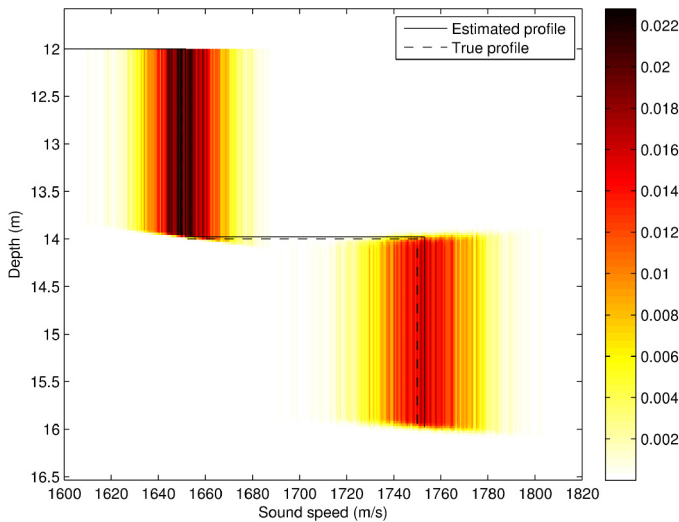


Fig. 5. Inversion results obtained by ISM for Config1. The true SSP (dashed line) and the median SSP estimated by ISM (solid line) are displayed over the marginal probability profile for the sediment SSP.

the water sound speed is added at the top of the seafloor structure. The third case is much more complex with a first “slow” layer and a “fast” layer embedded in a thick layer. In each case, the layer densities, required by specfem2D, are set to realistic values consistent with the layer sound speeds by the use of semi-empirical models [1].

The transmitted signal is a Ricker wavelet, with peak frequency set at 2500 Hz. Random white noise is added to the data with a high signal-to-noise ratio (see Fig. 4). For realistic results, we assume that we do not know the emitted signal, i.e., we cannot cross correlate.

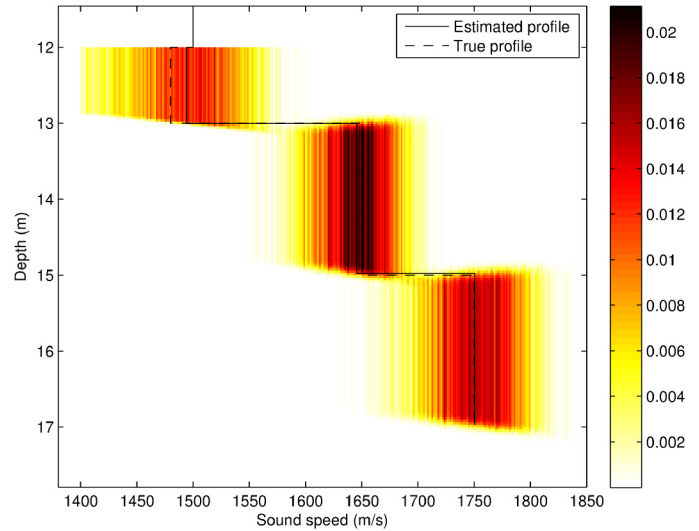


Fig. 6. Inversion results obtained by ISM for Config2. The true SSP (dashed line) and the median SSP estimated by ISM (solid line) are displayed over the marginal probability profile for the sediment SSP.

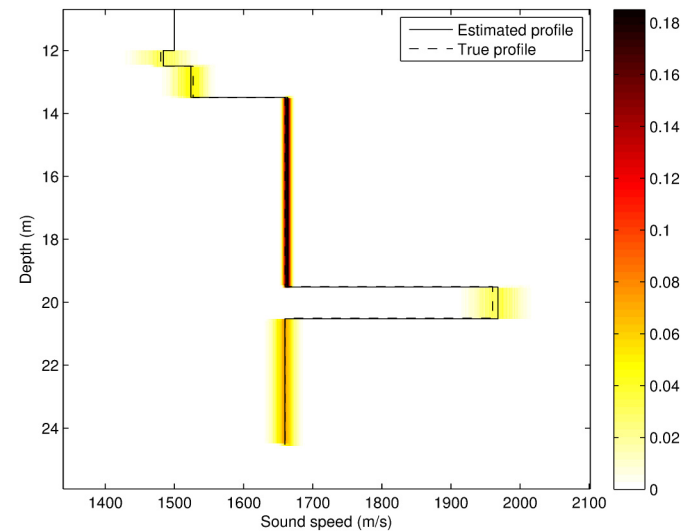


Fig. 7. Inversion results obtained by ISM for Config3. The true SSP (dashed line) and the median SSP estimated by ISM (solid line) are displayed over the marginal probability profile for the sediment SSP.

The inversion results obtained with ISM are displayed in Figs. 5–7. On each figure, the marginal PPD of the SSP is obtained using all positions of the virtual image sources collected in the Metropolis–Hastings sampling process (see Section III-B) with the median SSP estimated from the PPD. To obtain these results, the data standard deviation σ_t must be set which corresponds to the error made by the TKEO arrival-time

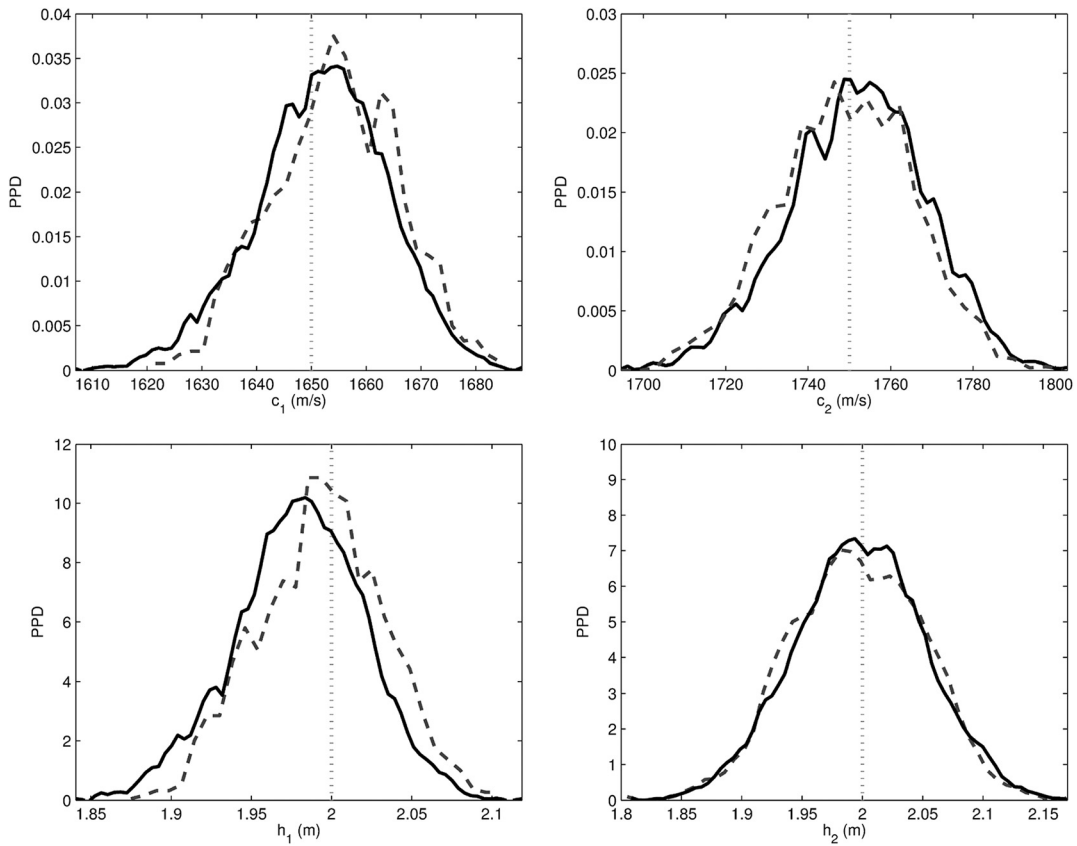


Fig. 8. Marginal probability densities for the parameters of Config1. The vertical dotted line represents the true value, the solid black curve is the result from ISM, and the gray dashed curve is the result from Bayesian travel-time inversion.

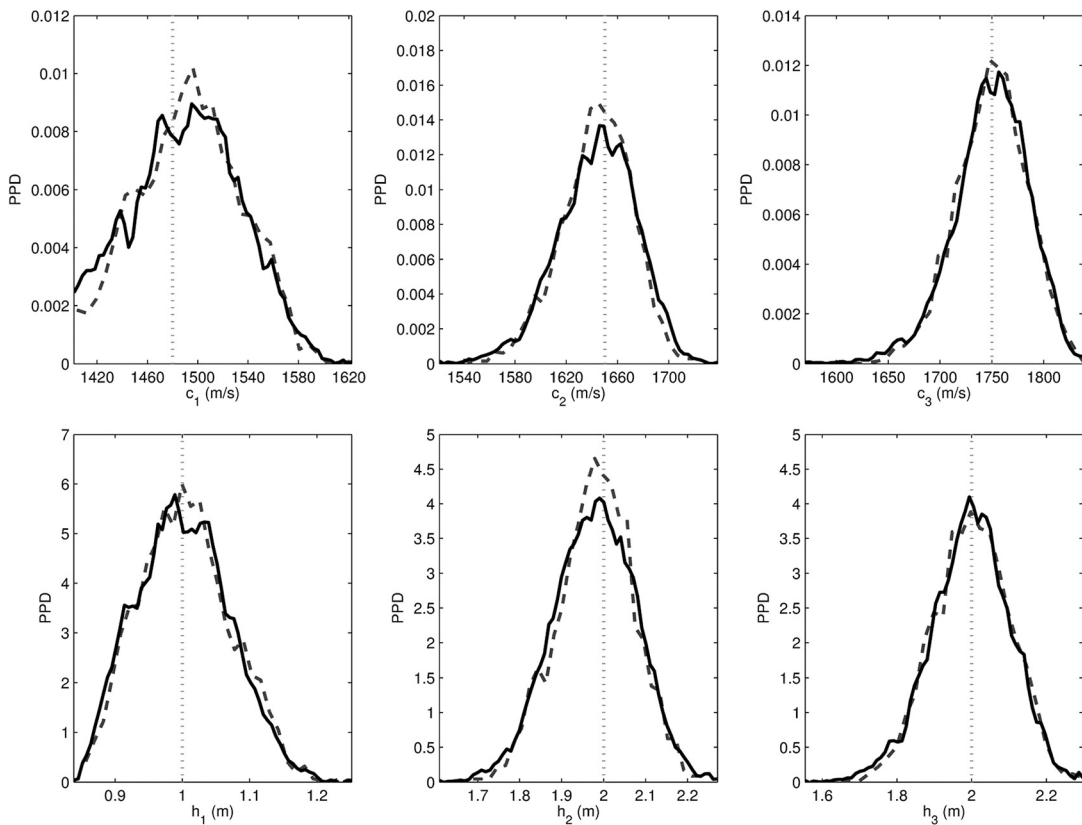


Fig. 9. Marginal probability densities for the parameters of Config2. The vertical dotted line represents the true value, the solid black curve is the result from ISM, and the gray dashed curve is the result from Bayesian travel-time inversion.

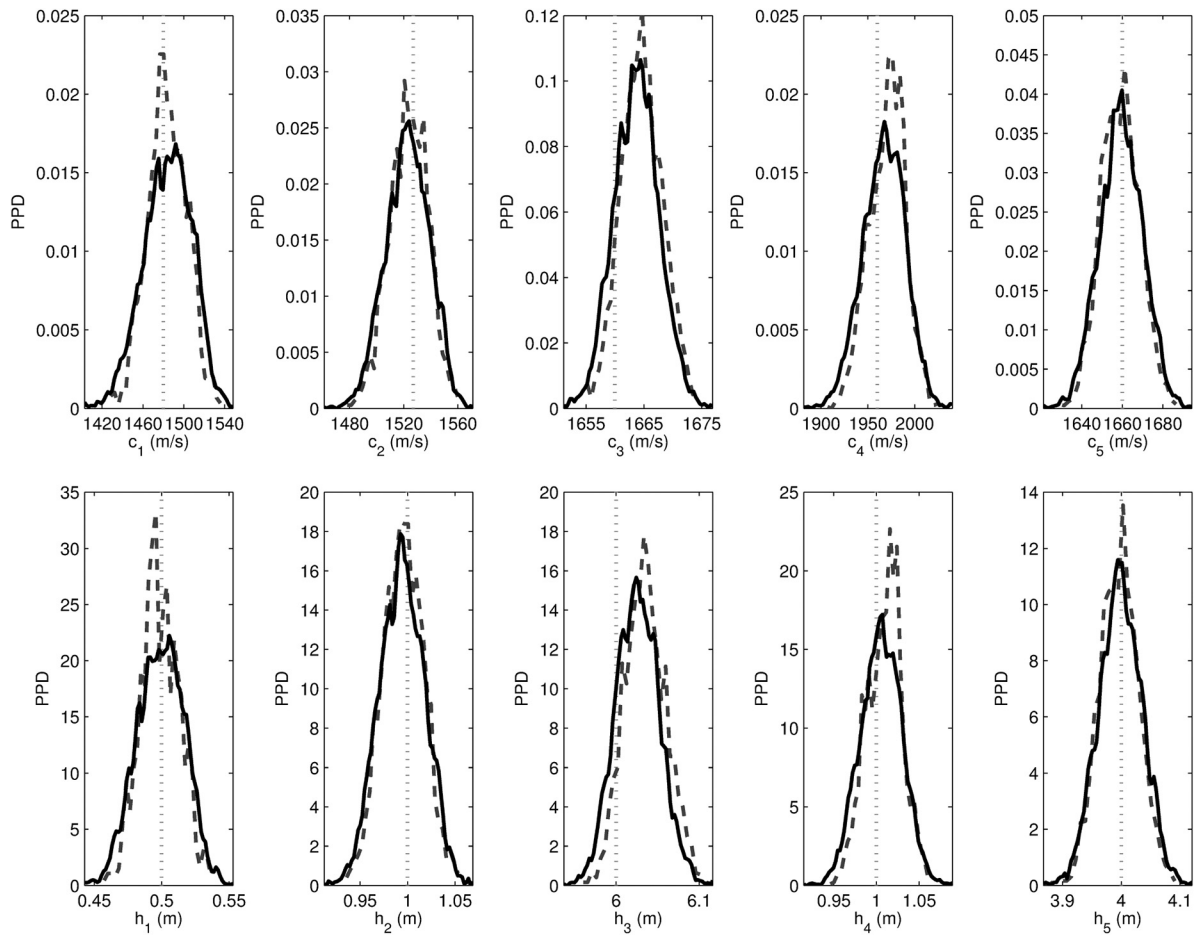


Fig. 10. Marginal probability densities for the parameters of Config3. The vertical dotted line represents the true value, the solid black curve is the result from ISM, and the gray dashed curve is the result from Bayesian travel-time inversion.

detection algorithm. The presented results are obtained assuming that the precision of this algorithm is five samples which is converted to σ_t using knowledge of the sampling frequency.

Based on these results, three remarks can be made on the Bayesian ISM. First, the overall quality of the inversion is very good. The algorithm is able to detect a thin layer with sound speed lower than sound speed in water (Fig. 7). However, working down the sediment column, the results are better for thicker layers. Second, despite the recursive nature of the ISM algorithm, there do not appear to be cumulative errors on the inverted SSP as a function of depth. For example, the results on Config3 (see Table I) show that even if the dispersion of the PPD of the first layer is relatively high, the SSP of the fifth layer is correctly estimated. These results confirm an analytical study on this subject [19]. Third, the Bayesian ISM algorithm is very efficient: it is fast and it gives simultaneously the median SSP and an estimation of the SSP uncertainty (from the sampled PPD). Even with quite complex sediment structure as Config3, the overall precision of the inversion is very satisfactory.

The same data set is used for a travel-time inversion scheme based on Metropolis–Hastings sampling [7]. In this approach, there are $N_s \times N_h$ data corresponding to the travel times from the layers to the hydrophones. The forward model involves efficient eigenray tracing in a layered environment using Newton’s method to determine the ray parameters [20]. The

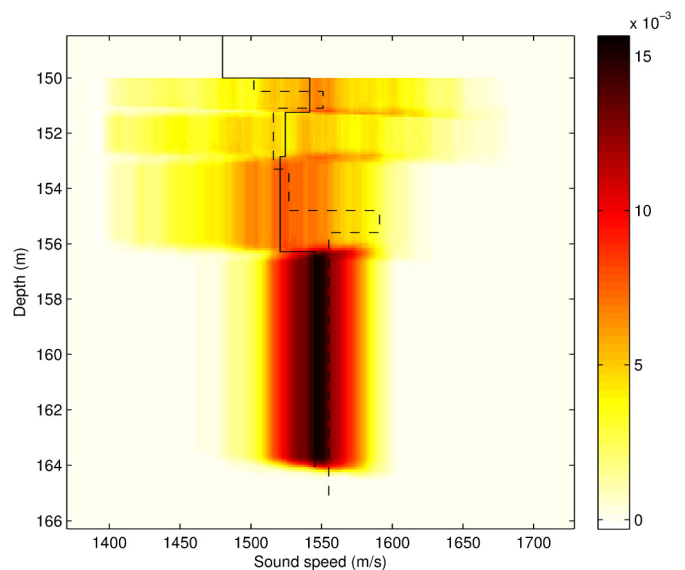


Fig. 11. PPD of the SSP inversion results obtained by ISM for SCARAB data. The solid line is the median SSP obtained by ISM and the dashed line is the SSP inverted by Holland and Osler [21].

results obtained are very similar to those from ISM but with computational times that are much longer, by a factor of about 20. Figs. 8–10 present the marginal densities of the estimated

TABLE II
GEOACOUSTIC INVERSION RESULTS FROM SCARAB DATA

Holland & Osler [21]			ISM-TK [5]			Bayesian ISM (median, Fig. 11)		
Layer	Depth (m)	Sound speed (m/s)	Layer	Depth (m)	Sound speed (m/s)	Layer	Depth (m)	Sound speed (m/s)
1	0.5	1502		
2	1.1	1551	I	1.4	1560	I	1.25	1541.7
3	3.3	1516	II	2.99	1517.9	II	2.85	1524.4
4	4.8	1527	III	6.44	1526.8	III	6.28	1520.8
5	5.6	1591		
6	15.1	1555	IV	14.19	1542.3	IV	14.07	1545.3

parameters for the three configurations obtained by ISM and travel-time inversion. For the two methods, the same convergence criterion was applied and the marginal densities are built with 5000 samples. The results are very similar.

B. At-Sea Experimental Data

The Bayesian ISM algorithm is tested on data acquired at sea during the Scattering And Reverberation from the sea Bottom (SCARAB) experiment near Elba Island off the west coast of Italy in 1998 [21]. The data were acquired at site 2 where the water depth is 150 m and the seabed is flat and featureless. The source is 200 m away from a vertical array, 64 m in length, moored to the seafloor. This array is composed of 15 hydrophones which are unevenly spaced. The lowermost hydrophone is about 12 m above the seafloor. Even if it is preferable to use horizontal array towed by a moving vehicle to be able to estimate geoacoustic parameters of range-dependent seafloors by ISM, we choose to use these data because they were already processed to test the image source method with Teager–Kaiser operator (ISM-TK) algorithm [5]. In that work, a correction of the array shape was performed, based on the detection of the direct path and the first reflected signal. The SSP estimation was achieved by a triangulation process of all the arrival times. In the present work, we use the arrival times detected by TKEO and the geometry estimated by Drira *et al.* [5]. We assume that the standard deviation of the errors made on the arrival times is equal to five samples. The PPD of the inverted SSP is shown in Fig. 11.

Estimated geoacoustic parameters are reported in Table II for the ISM-TK and Bayesian ISM inversion methods, and for Holland and Osler’s method [21] which exploits the data diversity (in time, space, and frequency) to build a joint time-frequency inversion algorithm. Ground truth, provided by sediment coring, is only available for the upper 15 m; comparisons are thus restricted to this depth. Since the Holland and Osler method compares favorably against the ground truth, it is used as the reference. Overall, our results are consistent with the findings of Holland and Osler (Table II). Compared to their results, only four layers are detected by TKEO and, therefore, the Bayesian ISM gives results for these four layers. The first layer in Holland and Osler’s work was not identified by the ISM due to the complexity of the sedimentary stratification of the first meters. The Bayesian ISM results are very close to the ISM-TK results but they have the advantage that they give

not only the median SSP of the seafloor but also quantitative uncertainty estimates. The Bayesian ISM results indicate that the thicker is the layer, the smaller are the uncertainties. For instance, the PPD of the second layer, which is about 1.6 m thick, is broader than the PPD of the fourth layer, which is about 7.8 m thick.

The uncertainties for this inversion are higher than those obtained for synthetic data. This could be due to the presence of a higher level of noise on the at-sea data which results in greater uncertainty in arrival times. Moreover, even though the array shape was corrected, this correction might be not perfect. Recent work on this subject [22] has shown that ISM, like other geoacoustic inversion methods, is very sensitive to the acquisition geometry and this problem should be investigated in more detail in future works.

VI. CONCLUSION

In this paper, we propose a Bayesian extension of the ISM for geoacoustic inversion. It is based on the use of the Teager–Kaiser energy operator to detect the arrival times of the signals emitted by the image sources and on the Metropolis–Hastings algorithm to sample their locations. After this step, the PPD of the SSP is computed with an inversion algorithm based only on the Snell–Descartes law of refraction. Thus, this approach keeps the simplicity of the ISM that makes this method fast but it includes the power of the Bayesian approach to estimate uncertainties.

The results obtained for both synthetic and measured data show the quality of this approach. The PPD of the inverted SSP is very similar to that obtained by Bayesian inversion of travel-time data which did not use the simplification of image sources. However, the Bayesian-ISM method is more efficient by at least an order of magnitude.

ACKNOWLEDGMENT

The measured data were kindly provided by C. Holland from the Applied Research Laboratory, Pennsylvania State University, University Park, PA, USA.

REFERENCES

- [1] D. Jackson and M. Richardson, *High-Frequency Seafloor Acoustics*, New York, NY, USA: Springer-Verlag, 2007.
- [2] X. Lurton, *An Introduction to Underwater Acoustics*, 2nd, New York, NY, USA: Springer-Verlag, 2010.

- [3] S. Pinson and L. Guillon, "Sound speed profile characterization by the image source method," *J. Acoust. Soc. Amer.*, vol. 128, no. 4, pp. 1685–1693, 2010.
- [4] S. Pinson, L. Guillon, and C. Holland, "Range dependent sediment sound speed profile measurements using the image source method," *J. Acoust. Soc. Amer.*, vol. 134, no. 1, pp. 156–165, 2013.
- [5] A. Drira, L. Guillon, and A. Boudraa, "Image source detection for geoacoustic inversion by the Teager-Kaiser energy operator," *J. Acoust. Soc. Amer. Exp. Lett.*, vol. 135, no. 6, pp. EL258–EL264, 2014.
- [6] A. Tolstoy, *Important Elements in: Geoacoustic Inversion, Signal Processing, and Reverberation in Underwater Acoustics*, Kerala, India: Research Signpost, 2008.
- [7] J. Detmer, S. E. Dosso, and C. W. Holland, "Uncertainty estimation in seismo-acoustic reflection travel time inversion," *J. Acoust. Soc. Amer.*, vol. 122, pp. 161–176, 2007.
- [8] S. Pinson, "Caractérisation des fonds marins par la méthode des sources images," Ph.D. dissertation, Université de Bretagne Occidentale, Brest, France, 2011.
- [9] J. F. Kaiser, "Some useful properties of Teager's energy operators," *Proc. Int. Conf. Acoust. Speech Signal Process.*, 1993, vol. 3, pp. 149–152.
- [10] A. Drira, L. Guillon, and A. Boudraa, "Geoacoustic inversion with image source method: Improvement of the detection algorithm," *Proc. 1st Int. Conf. Exhibit. Underwater Acoust.*, 2013, pp. 405–413.
- [11] A. Boudraa, J. Cexus, and K. Abed-Meraim, "Cross-psi-energy operator-based signal detection," *J. Acoust. Soc. Amer.*, vol. 132, pp. 4283–4289, 2008.
- [12] A. Savitzky and M. Golay, "Smoothing and differentiation of data by simplified least squares procedures," *Anal. Chem.*, vol. 8, pp. 1627–1639, 1964.
- [13] K. Mosegaard and A. Tarantola, "Probabilistic approach to inverse problems," *International Handbook of Earthquake and Engineering Technology*, New York, NY, USA: Academic, 2002.
- [14] S. E. Dosso and M. J. Wilmut, "Uncertainty estimation in simultaneous Bayesian tracking and environmental inversion," *J. Acoust. Soc. Amer.*, vol. 124, no. 1, pp. 82–97, 2008.
- [15] D. Komatitsch and J. P. Vilotte, "The spectral-element method: An efficient tool to simulate the seismic response of 2D and 3D geological structures," *Bull. Seismol. Soc. Amer.*, vol. 88, no. 2, pp. 368–392, 1998.
- [16] P. Cristini and D. Komatitsch, "Some illustrative examples of the use of a spectral-element method in ocean acoustics," *J. Acoust. Soc. Amer.*, vol. 131, no. 3, pp. EL229–EL235, 2012.
- [17] G. Jamet, C. Guennou, L. Guillon, C. Mazoyer, and J.-Y. Royer, "T-wave generation and propagation: A comparison between data and spectral element modeling," *J. Acoust. Soc. Amer.*, vol. 134, no. 4, pp. 3376–3385, 2013.
- [18] C. W. Holland, P. L. Nielsen, J. Dettmer, and S. Dosso, "Resolving meso-scale seabed variability using reflection measurements from an autonomous underwater vehicle," *J. Acoust. Soc. Amer.*, vol. 131, pp. 1066–1078, 2012.
- [19] S. Pinson, L. Guillon, and P. Cervenka, "Geoacoustic characterization by the image source method: A sensitivity study," *Proc. Acoust. Meeting*, Nantes, France, 2012, pp. 2809–2814.
- [20] S. E. Dosso and G. R. Ebbeson, "Array element localization and survey design," *Can. Acoust.*, vol. 33, pp. 16–26, 2005.
- [21] C. Holland and J. Osler, "High-resolution geoacoustic inversion in shallow water: A joint time- and frequency-domain technique," *J. Acoust. Soc. Amer.*, vol. 107, no. 3, pp. 1263–1279, 2000.
- [22] L. Guillon, S. E. Dosso, and N. R. Chapman, "Bayesian image source method for geoacoustic inversion," in *Seabed and Sediment Acoustics Meet.*, Bath, UK, 2015.



Laurent Guillon received the M.S. and Ph.D. degrees in acoustics from the University of Le Mans, Le Mans, France, in 1995 and 1999, respectively.

From 1999 to 2001, he worked as a Postdoctoral Student in the Laboratory for Mechanics and Acoustics (CNRS-LMA), Marseille, France. Since 2001, he has been an Associate Professor at the French Naval Academy, Brest, France. As a Visiting Professor, he spent six months in 2006 in the Applied Research Laboratory, Pennsylvania State University, University Park, PA, USA and six months at the

University of Victoria, Victoria, BC, Canada, in 2014. His research interests are in sediment acoustics, scattering modeling, geoacoustic inversion, and low-frequency propagation.

Dr. Guillon is a member of the Acoustical Society of America and the French Society of Acoustics.



Stan E. Dosso received the B.Sc. degree in physics and applied mathematics and the M.Sc. degree in physics from the University of Victoria, Victoria, BC, Canada, in 1982 and 1985, respectively, and the Ph.D. degree in geophysics from the University of British Columbia, Vancouver, BC, Canada, in 1990.

From 1990 to 1995, he worked in Ocean Physics (Arctic Acoustics) at the Defence Research Establishment Pacific, Victoria, BC, Canada. In 1995, he was appointed to an Ocean Acoustics Research Chair in the School of Earth and Ocean Sciences, University of Victoria, where he is currently a Professor. His research interests involve inverse problems in ocean acoustics and geophysics.

Dr. Dosso is a Fellow of the Acoustical Society of America and a member of the Canadian Acoustical Association (President 2003–2007) and the American Geophysical Union.



N. Ross Chapman (M'97–SM'03–F'10) received the Ph.D. degree in physics from the University of British Columbia, Vancouver, BC, Canada, in 1975.

He was the Group Leader of the Ocean Acoustics Group, Defence Research Establishment Pacific, Victoria, BC, Canada. In 1995, he was appointed Senior Chair in Ocean Acoustics at the University of Victoria, Victoria, BC, Canada. His research interests include acoustic and seismoacoustic propagation modeling, ambient noise in the ocean, and the development of inverse methods for localization and estimation of geoacoustic model parameters of the ocean bottom.

Dr. Chapman is a Fellow of the Acoustical Society of America. He is the Editor-in-Chief of the IEEE JOURNAL OF OCEANIC ENGINEERING.



Achraf Drira received the M.S. degree in acoustics from the University of Le Mans, Le Mans, France, in 2011. Currently, he is working toward the Ph.D. degree in signal processing and underwater acoustics at the French Naval Academy, Brest Cedex 9, France.

He is involved in the application of acoustics and signal processing tools for the analysis of geophysical and underwater acoustic signals. His research interests include image source method, Teager–Kaiser energy operator, time-frequency and time-scale analysis, multisensor processing, and

geoacoustic inversion.